https://doi.org/10.15407/ujpe66.9.803

E. OVODOK,[1] M. IVANOVSKAYA,[1] D. KOTSIKAU,[2] V. KORMOSH,[3] P. PYLYP,[4] V. BILANYCH[4]

[1] Research Institute for Physical-Chemical Problems of the Belarusian State University *(Minsk 220030, Belarus)*
[2] Belarusian State University *(Minsk 220030, Belarus)*
[3] Research Institute of Analytical Technique of Uzhhorod National University *(Uzhhorod 88000, Ukraine)*
[4] Department of Applied Physics, Uzhhorod National University *(Uzhhorod 88000, Ukraine)*

STRUCTURAL CHARACTERIZATION AND GAS SENSING PROPERTIES OF NANO-SIZED TIN DIOXIDE MATERIAL SYNTHESIZED FROM TIN(II) SULFATE

Structural features, surface condition, and gas-sensing properties of the nanocrystalline SnO_2 powders synthesized from $SnSO_4$ precursor by different methods have been studied. XRD, TEM, BET, and FTIR methods were used for the samples characterization. The gas sensors were fabricated by the thick-film technology from the synthesized SnO_2 powders. The responses of the sensors toward CO and CH_4 gases are measured. It is revealed that the preoxidation of $SnSO_4$ powder with concentrated sulfuric acid before the hydrolysis results in the lower particle size, higher surface area, improved adsorption activity, and higher sensitivity to reducing gases (CO, CH_4) of the synthesized SnO_2 materials, than in the case of the SnO_2 materials obtained without the preoxidation stage.

K e y w o r d s: SnO_2, $SnSO_4$, FTIR spectroscopy, thick-film sensor, CO, CH_4.

1. Introduction

Tin dioxide is widely used as a solid-state gas sensor material due to its physico-chemical properties, chemical stability, and relatively low cost [1–3]. The thick-film technology is extensively used for the fabrication of gas sensors [4–6]. A finely dispersed SnO_2 powder is required to obtain gas sensors of a good quality by the thick-film technology. N. Yamazoe and coworkers showed that the sensors fabricated from tin dioxide with particle sizes in the interval from 4 to 10 nm generally possess a higher gas sensitivity, than the sensors fabricated from coarser SnO_2 particles [7, 8].

One of the most commonly used methods for the production of SnO_2 materials is the sol-gel approach with a $SnCl_4$ solution as a precursor [9–11]. However, N. Yamazoe revealed that using $SnCl_4$ precursor within the unmodified sol-gel method does not provide the possibility to obtain an SnO_2 powder calcinated at 600 °C with the sizes of particles smaller than 15 nm [7]. C. Xu and coworkers showed that the crystallite size of SnO_2 can be stabilized against the thermal growth, when the stannic acid gel was impregnated with a small amount (5 at. %) of a foreign metal oxides [8]. In our work, we suggest the SnO_2 synthesis route that allows stabilizing the SnO_2 crystallite size during a thermal treatment without adding extraneous metal oxides.

G.W. Wang and coworkers showed that the addition of SO_4^{2-} ions to tin(IV) hydroxide during the SnO_2 synthesis from $SnCl_4$ caused a notable increase in the surface area of the calcinated oxide [12]. However, the residual chloride ions can degrade the gas- sensitive properties of the SnO_2 sensor materials. H.C. Chiu and C.S. Yeh showed that the presence of Cl^- ions change the number of the oxygen species in SnO_2 and decrease the sensitivity of the sensor to ethanol [13]. Thus, using tin sulfate salts as a precursor is reasonable. The presence of Sn(IV) ions in a solution is necessary for the formation of sols, which allows one to get SnO_2 thin film samples and fine dispersed SnO_2 powders. However, tin(IV) sulphate

is easily hydrolyzed by crystal water and humidity of air. For this reason, $SnSO_4$ salt was chosen as an initial precursor.

In addition, sulphate ions can modify the surface and change the adsorption and catalytic properties of metal oxides. K. Arata and M. Hino found that SnO_2, TiO_2, and ZrO_2 calcinated oxides, which were synthesized in the presence of sulphate ions, are characterized by a high concentration of acid centers. The ratio between Lewis and Bronsted acid sites on these oxides can change under a moisture treatment [14]. Surface acid sites influence the catalytic activities of materials. The surface sulfate groups can be directly involved in the process of gas adsorption, or they can act as an activator of reagents in catalytic reactions. An improvement of the sensitivity of Fe_2O_3–SnO_2 materials to CH_4 under the influence of SO_4^{2-} ions has been established by M. Takana and coworkers [15].

The present work is aimed at the characterization of the structure and gas-sensing properties of SnO_2 materials that are prepared by different routes from the $SnSO_4$ precursor and are suitable for the production of thick film gas sensors.

2. Material and Methods

Two methods of synthesis of a SnO_2 powder from the $SnSO_4$ precursor were used.

Method I. The SnO_2 powder was obtained by the hydrolysis of a $SnSO_4$ solution and a subsequent thermal treatment of the precipitated oxyhydroxide. Here, 100 ml of a $SnSO_4$ solution (C = 50 g/l) was prepared by dissolving the freshly recrystallized $SnSO_4$ salt in distilled water acidified with sulfuric acid (pH 2). An ammonia solution (C = 5 wt. %) was added dropwise to a $SnSO_4$ solution until pH 8 was reached.

The obtained precipitate was separated by the centrifugation and washed 3 times with distilled water. 50 ml of distilled water and 0.1 ml of concentrated sulfuric acid were added to the precipitate. Then the suspension was ultrasonificated (f = 22 kHz, P = = 130 W) for 2 min. The resultant precipitate was dried at 50 °C and calcinated for 1 h at 600 °C (SnO_2(I)).

Method II. The preoxidation of $SnSO_4$ salt with concentrated sulfuric acid was carried out before the hydrolysis. Typically, 5 g of the freshly recrystallized $SnSO_4$ powder was added to 5.5 ml of concentrated H_2SO_4 acid. The suspension was heated at 200°C during 10 min. At the end of the reaction, the solution was diluted with distilled water up to 100 ml. Then an ammonia solution (C = 5%) was added dropwise until pH 8 was reached.

The obtained precipitate was separated by the centrifugation and washed 3 times with distilled water. 50 ml of distilled water and 0.1 ml of concentrated sulfuric acid were added to the precipitate. Then the suspension was ultrasonificated (f = 22 kHz, P = = 130 W) for 2 min. A transparent sol was obtained under such treatment. The resultant sol was dried at 50 °C and calcinated at 600 °C (SnO_2(II)). Method II was developed by us for obtaining a highly dispersed calcinated SnO_2 powder.

The phase composition of the materials was characterized by the X-ray diffraction (XRD) analysis. The XRD analysis was carried out on a PANalytical X'Pert PRO MRD (multipurpose research diffractometer, Holland) with a modular construction using Cu K_α–radiation. The fine structural features of the SnO_2 crystallites were revealed by the transmission electron microscopy (TEM). The TEM examinations were performed on a *LEO 906E* transmission electron microscope. The specific area ($S_{\rm BET}$) was calculated by the BET (Brunauer–Emmett–Teller) method from nitrogen adsorption isotherms measured by a Gemini V2.00 surface analyzer (Micromeritics Instrument Corp.) at –196 °C. The state of the surface of samples was examined by the Fourier transform infrared spectroscopy (FTIR). The FTIR analysis was carried out on an AVATAR FTIR-330 spectrometer supplied with a smart diffuse reflectance accessory in the wavenumber range from 400 to 4000 cm^{-1}.

The gas sensors were fabricated by the thick-film technology. The SnO_2 powders were grinded thoroughly with ethanol in an agate mortar. Then the obtained paste was deposited onto polycrystalline Al_2O_3 substrates ($1.6\times1.6\times0.25$ mm^3) supplied with a Pt interdigitated electrode on the front side and a Pt-heater on the rear side. The sensor elements were annealed at 570 °C for 3 h in air. The thickness of the oxide sensitive layer was about 15 mkm.

SnO_2(I) and SnO_2(II) sensors were fabricated from the SnO_2 powders synthesized by methods I and II, respectively. A contact electric potential was applied to the heater, and a resistance of the sensing layer was measured in air ($R_{\rm air}$) and in air-gas mixtures

(R_{gas}). The sensor response (G) was calculated as R_{air}/R_{gas}. The response measurements were carried out in air-gas mixtures with a CH_4 concentration of 1000 ppm and with a CO concentration of 1000 ppm (30% relative humidity) at different working temperatures. Concentration dependences of the resistances ofsensors at the CO detection were obtained at determined optimal operation temperatures.

3. Results and Discussion

3.1. Structure, morphology, and surface state

The X-ray diffraction patterns of the as-prepared and the annealed at 600 °C samples are shown in Fig. 1. The structural parameters of the samples are summarized in Table. According to the XRD data, the as-prepared sample synthesized by method I contains the $Sn_6O_4(OH)_4$ phase (JCPDS 84-2157) and SnO_2 rutile phase (JCPDS 88-0287).

The as-prepared sample synthesized by method II is characterized by wide diffraction peaks assigned to the SnO_2 rutile phase (JCPDS 88-0287). The rutile phase predominates in the all samples calcinated at 600 °C. Traces of the SnO phase were additionally observed in the SnO_2(I) sample. The width of diffraction peaks in the patterns of the SnO_2(II) sample is much higher, than in the case of SnO_2(I) sample. The average size of the rutile SnO_2 crystallites was estimated by the Debye–Scherrer equation from the width of the (110) reflexion. The SnO_2(I) sample is characterized by an average crystallite size of about 24 nm. The SnO_2(II) sample consists from smaller crystallites (5.5 nm). The lattice parameters were calculated for the calcinated SnO_2 samples. The unit cell parameters of the SnO_2(I) sample correspond well to the reference data (a = 0.4738 nm, c = 0.3187 nm) [16]. In contrast, the a parameter of the SnO_2(II) sample is slightly lower (0.4723 nm), and the c parameter is slightly higher (0.3199 nm), than the values given in the literature [16]. The formation of a defective lattice is caused by the influence of sulphate groups under the dehydration and crystallization processes of initial particles during the synthesis of the SnO_2(II) sample.

According to the TEM data, the SnO_2(I) and SnO_2(II) samples are polycrystalline (Fig. 2). The particles have a similar morphology close to the spherical one. However, they are characterized by different sizes. The particle size estimated for the SnO_2(II) sample is 5.5 nm, and that for the SnO_2(I) sample is 27 nm. The TEM data are in agreement with the crystallite size calculated from XRD patterns.

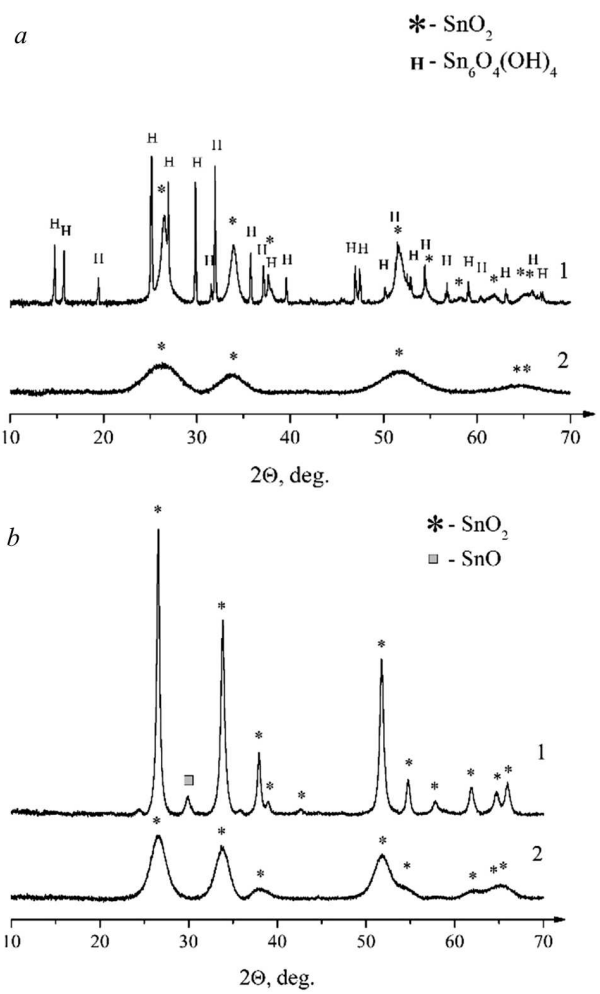

Fig. 1. X-ray diffraction patterns of as-prepared (*a*) and calcinated at 600 °C (*b*) samples synthesized by method I (*1*) and method II (*2*)

The specific surface area of the samples was measured by means of the BET analysis, which shows that the surface areas are 17.9 m^2/g and 70.4 m^2/g for SnO_2(I) and SnO_2(II) powders, respectively. Thus, method II allows one to synthesize a SnO_2 powder, which is characterized by a high surface area and a low crystallite size after the calcination at 600 °C.

The described structural differences of the SnO_2 samples are determined by the chemical processes, which take place during the syntheses.

Structural characteristics of the SnO_2 samples synthesized from $SnSO_4$ by methods I and II

Method of synthesis	Phase composition of as-prepared samples	Phase composition of samples calcinated at 600 °C	d_{aver}, nm (XRD)	a parameter, nm	c parameter, nm	d_{aver}, nm (TEM)	Specific surface area, m^2/g (BET)
Method I	$Sn_6O_4(OH)_4$ SnO_2	SnO_2 SnO	24±1	0.4738	0.3187	27	17.9
Method II	$SnO_2 \cdot xH_2O$	SnO_2	5.5±1	0.4723	0.3199	5.5	70.4

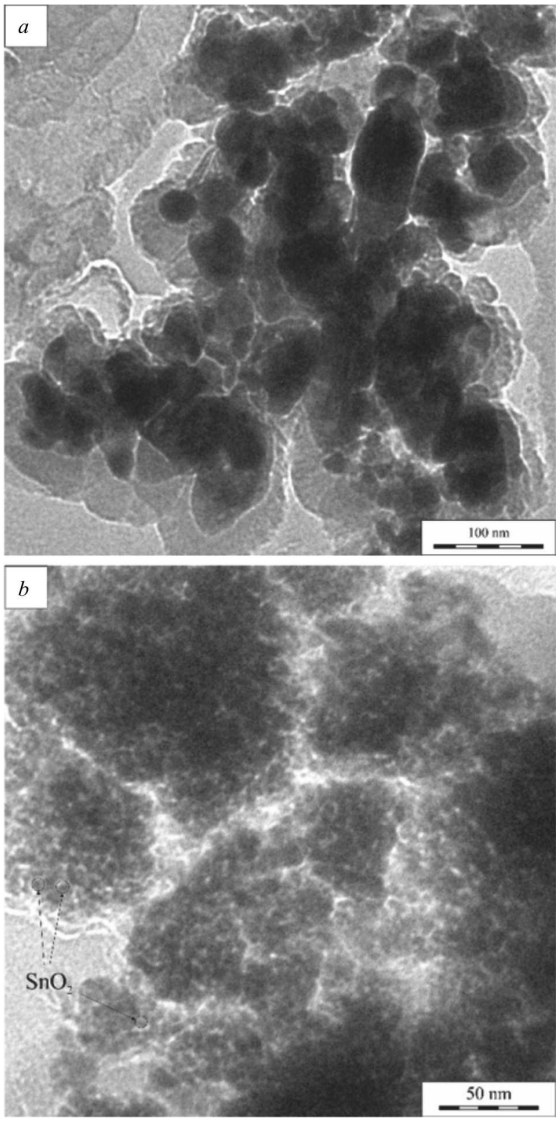

Fig. 2. TEM images of the SnO_2 samples (600 °C) synthesized by (*a*) method I and (*b*) method II

In method I, tin(II) oxyhydroxide is precipitated by the hydrolysis of $SnSO_4$ with an ammonia solution (Eq. (1))

$$6Sn^{2+} + 6SO_4^{2-} + 12NH_4^+ + 12OH^- \longrightarrow$$
$$\longrightarrow Sn_6O_4(OH)_4 \downarrow + 12NH_4^+ + 6SO_4^{2-} + 4H_2O. \quad (1)$$

The $Sn_6O_4(OH)_4$ crystalline phase with traces of the SnO_2 rutile phase is observed in the dried precipitate. Ultrasonification during the synthesis induces a partial decomposition and the oxidation of tin(II) oxyhydroxide to SnO_2. According to FTIR data, a certain amount of SO_4^{2-} groups is preserved on the surface of $Sn(OH)_2$ particles after the drying (Fig. 3, *a*). Then tin(II) oxyhydroxide decomposes to SnO and oxidizes to SnO_2 under the heating up to 600 °C.

In method II, Sn^{2+} ions are oxidized to Sn^{4+} ions by concentrated sulfuric acid at the first stage of the synthesis (Eq. (2) and (3))

$$Sn^{2+} - 2e \longrightarrow Sn^{4+}, \quad (2)$$
$$2H^+ + H_2SO_4 + 2e \longrightarrow SO_2 + 2H_2O. \quad (3)$$

After this treatment, Sn^{4+} and SO_4^{2-} ions, as well as traces of non-oxidized Sn^{2+} ions, present in the resultant solution. The amount of the remained Sn^{2+} ions can be varied by the duration of the heating. A polymerized tin oxyhydroxide is formed during the hydrolysis of Sn^{4+} ions by an ammonia solution (Eq. (4))

$$Sn^{4+} + 4OH^- \rightarrow SnO_2 \cdot 2H_2O. \quad (4)$$

The product consists of polynuclear complexes interconnected by bridging OH-groups, in which H_2O molecules are located in the coordination environment of tin ions. In the core of the generated particles, tin atoms have coordination of oxygen atoms

similar to SnO_2 oxide. Hydroxyl groups and hydrogen bonded water molecules cover the SnO_2 core. Sulfate ions are intercalated in these particles and coordinated by tin ions. Annealing the sample at 600 °C induces the dehydration of the initial particles and the crystallization and growth of tin dioxide crystallites.

FTIR spectra illustrated in Fig. 3 show that sulfate ions are observed in both $SnO_2{\cdot}2H_2O$ and $Sn_6O_4(OH)_4$ precipitates after the washing and drying. However, as-prepared SnO_2(I) and SnO_2(II) samples are characterized by quantitative and qualitative differences in the interval of the vibrational mode of $[SO_4]^{2-}$ groups.

A free sulfate ion is characterized by the T_d symmetry. Two vibrational modes (ν_3 and ν_4) of four fundamental oscillations are active in IR spectroscopy. When sulfate ions are bounded with particles, their symmetry decreases from T_d to C_{2V} or C_{3V}, and additional bands can appear in IR spectra. The vibrational modes of bidentate bonded sulfate groups are observed in the IR spectra of the as-prepared SnO_2(I) sample: $\nu_1 = 948$ cm^{-1}, $\nu_3 = 1015$, 1115, 1246 cm^{-1}, and $\nu_4 = 605$, 661 cm^{-1} [17]. The bands assigned to $\nu_1 = 948$ cm^{-1}, $\nu_3 = 1027$, 1105, and a shoulder at 1182, ν_4 = shoulders at 600 and 642 cm^{-1} vibrations of bidentate bonded $[SO_4]^{2-}$ groups are detected in the FTIR spectra of the as-prepared sample synthesized by method II. The frequencies of the bands vary from sample to sample due to the difference in the energy state of surface tin atoms, which coordinate sulfate groups.

The intensities of the ν_1 and ν_3 vibrational modes of $[SO_4]^{2-}$ group are considerably higher for the as-prepared SnO_2(II) sample, than for the as-prepared SnO_2(I) sample. This is due to a higher sorption capacity of the particles in a sol, than in a precipitate. In the case of the sol, sulfate ions can be incorporated in the micelle structure and remain in the structure during the subsequent drying of the sample (Eq. (5))

$$\{(SnO_2{\cdot}nH_2O)_m{\cdot}2xH^+{\cdot}(x-y)SO_4^{2-}\}^{2y+}{\cdot}ySO_4^{2-}. \quad (5)$$

The IR spectra of the as-prepared samples show the absorbance in the interval from 2500 to 3750 cm^{-1}. This broad band is assigned to the stretching OH vibrations in hydroxyl groups and adsorbed water (ν(OH)) [17]. The band at 1660 cm^{-1} characterizes the deformation HOH vibrations (δ(HOH)). The intensity and width of the ν(OH) bands are noticeably

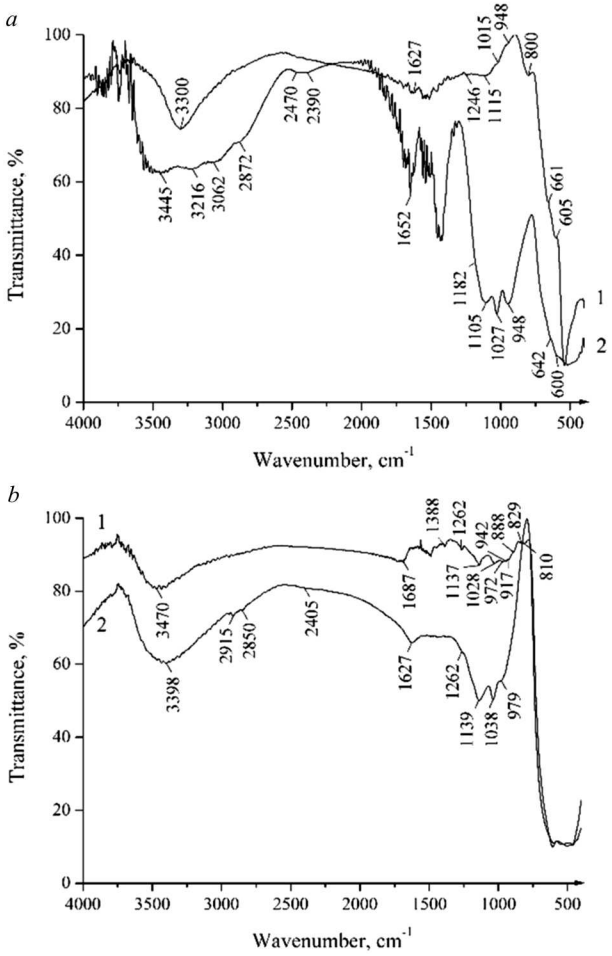

Fig. 3. FTIR spectra of as-prepared (*a*) and calcinated at 600 °C (*b*) samples synthesized by method I (*1*) and method II (*2*)

higher for the as-prepared SnO_2(II) sample, than for the as-prepared SnO_2(I) sample. Furthermore, the local maxima of the absorption at 3445, 3216, 3062, and 2872 cm^{-1} in the band of ν(OH) vibrations and additional bands for δ(HOH) vibrations are observed in the IR spectrum of the as-prepared SnO_2(II) sample. The features of the spectrum related to the position of the ν(OH) and δ(OH) vibrations indicate the formation of hydrogen bonds between SO_4^{2-} and OH-groups. In addition, the presented IR data confirm the assumption that sulfate ions are incorporated in the micelle structure of $SnO_2{\cdot}nH_2O$ hydrosol.

The $\nu[SO_4]^{2-}$ bands have a low intensity in the FTIR spectrum of the calcinated SnO_2(I) sample, whereas a high intensity of these bands is revealed

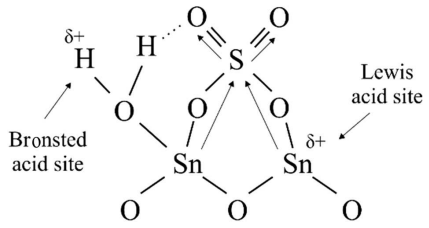

Fig. 4. Scheme of acid centers on SnO_2 surface modified with sulphate groups

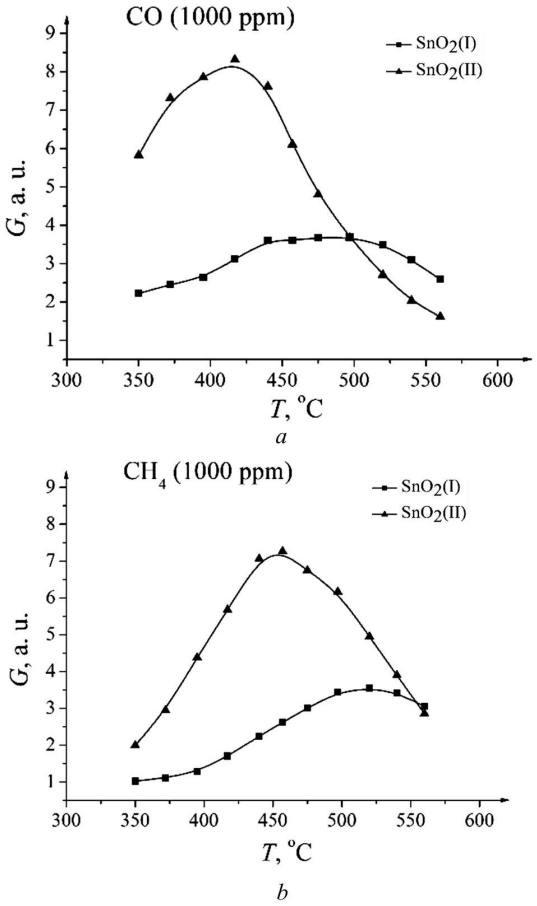

Fig. 5. The dependences of response vs working temperature for SnO_2 (I and II) sensors at the detection of CO (1000 ppm) (*a*) and CH_4 (1000 ppm) gases (*b*)

in the spectrum of the SnO_2(II) sample after the calcination (see Fig. 3, *b*). The triplet of $[SO_4]^{2-}$ vibrational bands is observed for the calcinated SnO_2(II) sample, but the maxima of the bands are shifted to higher wavenumbers (979, 1038, 1139 cm^{-1}) comparing to the as-prepared sample. Moreover, in the

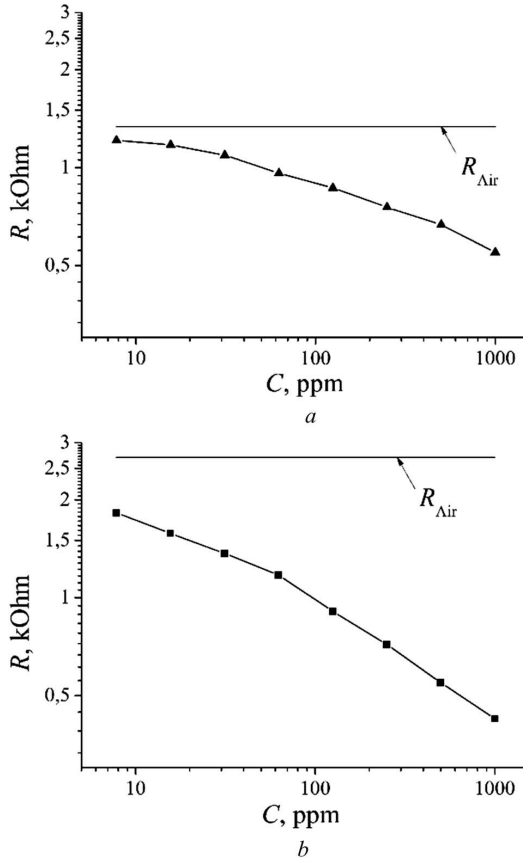

Fig. 6. Dependences of the electric resistance of SnO_2 (I) sensor (*a*) and SnO_2 (II) sensor (*b*) on the concentration of CO in air

spectrum of the SnO_2(II) sample annealed at 600 °C, a wide band attributed to ν(OH) vibrations is observed. Note that the local maxima are resolved less in this interval, than for the as-prepared sample. The adsorption maximum of the ν(OH) band is observed at 3470 cm^{-1}, and the small peaks are detected at 2915, 2855, 2405 cm^{-1}. These peaks indicate that hydrogen-bonded OH groups are presented on the oxide surface. The interaction between SO_4^{2-}-ions and OH-groups influences the state of the surface adsorption centers of SnO_2 oxide.

Thus, according to the IR data, the surfaces of the SnO_2(I) and SnO_2(II) samples contain unequal amounts of $[SO_4]^{2-}$ groups. The as-prepared SnO_2(II) sample has a high amount of surface hydroxyl groups and adsorbed water, which forms hydrogen bonds with $[SO_4]^{2-}$ groups. Furthermore, sulphate groups are included directly in the micelle

structure. Sulphate groups influence the processes of dehydration and crystallization of oxide. As a result, the SnO_2(II) sample calcinated at 600 °C is characterized by a low particle size and a high surface area and contains a high amount of surface sulfate groups. The sulphate groups are bidentates bound with tin cations. Surface SO_4^{2-} ions create Bronsted acid sites and improve acceptor properties of the surface Sn^{4+} lattice cations (Lewis acid sites) due to the inductive interaction (Fig. 4). Surface acid sites are active in the adsorption and dissociation of gas molecules. Kustov and coworkers showed that the modification of ZrO_2 with SO_4^{2-} anions results in a strengthening of the surface Lewis acid sites represented by low-coordinated zirconium ions, which promotes the adsorption of CO molecules [18].

Gas-sensing properties

We now consider the gas-sensing properties of SnO_2 thick-film sensors. In order to determine the optimum operating temperatures, the response of the sensors to CO and CH_4 (1000 ppm) are tested as a function of the operating temperature, as shown in Fig. 5. The response of the SnO_2(II) sensor to CO and CH_4 is about 2.5 times higher, than the response of the SnO_2(I) sensor over a wide interval of working temperatures (see Fig. 5, *a, b*). The response maxima of the SnO_2(II) sensor to both gases are observed at lower temperatures, than iforn the SnO_2(I) sensor. The former has the maximum response to CO at a lower operation temperature, than to CH_4. In the interval of temperatures from 350 to 375 °C, the highest difference between the responses of the SnO_2(II) sensor to CO and CH_4 is observed. This operation mode is suitable for the selective detection of carbon monoxide.

Further, we measured changes in the sensor resistance at different concentrations of CO at the optimal operation temperature. Figure 6 shows the dependences of the electric resistance of the sensors on the concentration of CO in air. The SnO_2(II) sensor is characterized by a higher sensitivity to CO as compared with the SnO_2(I) sensor. Carbon monoxide can be detected by the SnO_2(II) sensor at concentrations smaller than 10 ppm.

The gas-sensing properties of the SnO_2(II) sensor are caused, on the one hand, by structural features of the SnO_2 powder. The small size of SnO_2 particles (d = 5.5 nm), which is comparable with the doubled thickness of the space-charge layer ($L \approx 3$ nm) [7], provides a high sensitivity of the SnO_2(II) sensor to reducing gases. The high surface area of the powder promotes the absorption of gases. On the other hand, surface sulfate groups increase the strength of the Lewis acid sites and promote the CO adsorption on the oxide surface.

4. Conclusions

SnO_2 powders were synthesized from tin(II) sulphate by different routes. The preoxidation of a $SnSO_4$ powder with concentrated H_2SO_4 prior to the hydrolysis stage allowed us to obtain the SnO_2 powder, which is characterized by the 5.5-nm average particle size and a high surface area (70.4 m^2/g) after the calcination at 600 °C. The high concentration of SO_4^{2-} groups is observed on the surface of this sample. The thick-film SnO_2(II) gas sensor is characterized by a higher response to CO and CH_4 gases and a lower optimal working temperature as compared to the SnO_2(I) sensor. The SnO_2(II) sensor can be used for the detection of CO concentrations smaller, than 10 ppm. The improvement of the gas sensing properties of tin(IV) oxide layers is caused by their structural features and the effect of SO_4^{2-} ions on the adsorption properties of the oxide surface.

This work was performed within the framework of an international Ukrainian-Belarusian grant (Belarusian RFFR grants No. X21УКРГ-002).

1. M. Batzill, U. Diebold. The surface and materials science of tin oxide. *Prog. Surf. Sci.* **79**, 45 (2005).
2. W. Göpel, K.D. Schierbaum. SnO_2 sensors: current status and future prospects. *Sens. Actuator B Chem.* **26**, 1 (1995).
3. D. Kohl. Surface processes in the detection of reducing gases with SnO_2-based devices. *Sens. Actuator.* **18**, 71 (1989).
4. G. Martinelli, M. C. Carotta. Thick-film gas sensors. *Sens. Actuator B Chem.* **23**, 157 (1995).
5. S.P. Patil, V.L. Patil, S.S. Shendage, N.S. Harale, S.A. Vanalakar, J.H. Kim, P.S. Patil. Spray pyrolyzed indium oxide thick films as NO_2 gas sensor. *Ceram. Int.* **42**, 16160 (2016).
6. D.C. Pugh, S.M. Hailes, I.P. Parkin. A gas-sensing array produced from screen-printed, zeolite-modified chromium titanate. *Meas. Sci. Technol.* **26**, 085102 (2015).
7. N. Yamazoe. New approaches for improving semiconductor gas sensors. *Sens. Actuator B Chem.* **5**, 7 (1991).

8. C. Xu, J. Tamaki, N. Miura, N. Yamazoe, Grain size effects on gas sensitivity of porous SnO_2-based elements. *Sens. Actuator B Chem.* **3**, 147 (1991).
9. S.M. Badalyan, M.N. Rumyantseva, S.A. Nikolaev, A.V. Marikutsa, V.V. Smirnov, A.S. Alikhanian, A.M. Gaskov. Effect of Au and NiO catalysts on the NO_2 sensing properties of nanocrystalline SnO_2, *Inorg. Mater.* **46**, 232 (2010).
10. D. Wang, Y. Chen, Z. Liu, L. Li, C. Shi, H. Qin, J. Hu. CO_2-sensing properties and mechanism of nano-SnO_2 thick-film sensor. *Sens. Actuator B Chem.* **227**, 73 (2016).
11. K. Suematsu, K. Yamada, M. Yuasa, T. Kida, K. Shimanoe. Evaluation of Oxygen Adsorption Based on the Electric Properties of SnO_2 Semiconductor Gas Sensors. *Sensor. Mater.* **28**, 1211 (2016).
12. G.W. Wang, H. Hattori, K. Tanabe. The enhancement of acid strength and catalytic activity of SnO_2 by the addition of sulfate ion. *Chem. Lett.* **12**, 277 (1983).
13. H.C. Chiu, C.S. Yeh. Hydrothermal synthesis of SnO_2 nanoparticles and their gas-sensing of alcohol. *J. Phys. Chem. B* **111**, 7256 (2007).
14. K. Arata, M. Hino. Preparation of superacids by metal oxides and their catalytic action. *Mater. Chem. Phys.* **26**, 213 (1990).
15. M. Takano, Y. Bando, N. Nakanishi, M. Sakai, H. Okinaka. Characterization of fine particles of the α-Fe_2O_3-SnO_2 system with residual SO_4^{2-} ions on the surface. *J. Solid State Chem.* **68**, 153 (1987).
16. A.A. Bolzan, C. Fong, B.J. Kennedy, C.J. Howard. Structural studies of rutile-type metal dioxides. *Acta Crystallogr. Sect. B* **53**, 373 (1997).
17. K. Nakamoto. *Infrared and Raman Spectra of Inorganic and Coordination Compounds* (John Wiley & Sons, Ltd. 1986).
18. L.M. Kustov, V.B. Kazansky, F. Figueras, D. Tichit. Investigation of the acidic properties of ZrO_2 modified by SO_4^{2-} anions. *J. Catal.* **150**, 143 (1994).

Received 24.12.20

Е.А. Оводок, М.И. Ивановская, Д.А. Котиков, В.В. Кормош, П.П. Пилип, В.С. Биланич

СТРУКТУРНІ ХАРАКТЕРИСТИКИ І ГАЗОЧУТЛИВІ ВЛАСТИВОСТІ НАНОРОЗМІРНИХ МАТЕРІАЛІВ ДІОКСИДУ ОЛОВА, СИНТЕЗОВАНИХ ІЗ СУЛЬФАТУ ОЛОВА

Досліджено структурні особливості, стан поверхні та газочутливі властивості нанокристалічних порошків SnO_2, синтезованих із прекурсора $SnSO_4$ різними методами. Для вимірювання характеристик зразків використовувалися методи XRD, TEM, BET і FTIR. Газові сенсори виготовлялися за товстоплівковою технологією з синтезованих порошків SnO_2. Проведено вимірювання реакції отриманих датчиків на гази CO і CH_4. Виявлено, що попереднє окислення порошку $SnSO_4$ концентрованою сірчаною кислотою перед гідролізом приводить до меншого розміру частинок, більшої площі поверхні, поліпшеної адсорбційної активності і більшої чутливості до відновних газів (CO, CH_4) синтезованих матеріалів SnO_2, ніж у випадку матеріалів SnO_2, отриманих без стадії попереднього окислення.

Ключові слова: SnO_2, $SnSO_4$, спектроскопія FTIR, товстоплівковий датчик, CO, CH_4.